nature electronics

ARTICLES

https://doi.org/10.1038/s41928-021-00545-5

Check for updates

An electrically conductive silver–polyacrylamide–alginate hydrogel composite for soft electronics

Yunsik Ohm[1,2,5], Chengfeng Pan[1,2,5], Michael J. Ford[1,2], Xiaonan Huang[1,2], Jiahe Liao[1,3] and Carmel Majidi[1,2,3,4] ✉

Hydrogels offer tissue-like compliance, stretchability, fracture toughness, ionic conductivity and compatibility with biological tissues. However, their electrical conductivity (<100 S cm^{-1}) is inadequate for digital circuits and applications in bioelectronics. Furthermore, efforts to increase conductivity by using hydrogel composites with conductive fillers have led to compromises in compliance and deformability. Here, we report a hydrogel composite that has a high electrical conductivity (>350 S cm^{-1}) and is capable of delivering direct current while maintaining soft compliance (Young's modulus < 10 kPa) and deformability. Micrometre-sized silver flakes are suspended in a polyacrylamide–alginate hydrogel matrix and, after going through a partial dehydration process, the flakes form percolating networks that are electrically conductive and robust to mechanical deformations. To illustrate the capabilities of our silver–hydrogel composite, we use the material in a stingray-inspired swimmer and a neuromuscular electrical stimulation electrode.

Soft electronics that exhibit high electrical conductivity and match the compliance of biological tissue are important in the development of wearable computing[1,2], soft sensors[3,4] and actuators[5], energy storage/generation devices[6,7] and stretchable displays[8,9]. A variety of material architectures have been used to create soft and stretchable electronics, including deterministic (such as wavy or serpentine) structures[10,11], soft microfluidic channels[12,13] and conductive composites or polymers[14–16]. However, these conductive materials have intrinsic limitations, such as relatively high Young's modulus (≫1 MPa in some cases) or limited deformability, and are not ideally suited for applications related to bioelectronic systems (such as those that require interfacing with biological tissues). Recently, researchers have demonstrated conductive elastomers with enhanced stretchability and compliance by incorporating microdroplets of liquid metal alloys such as eutectic gallium indium (EGaIn)[17,18]. In particular, a highly stretchable and conductive polymer composite has been developed using silver and EGaIn particles embedded in an ethylene vinyl acetate copolymer[18]. Although EGaIn-based polymer composites exhibit an encouraging combination of high conductivity, stretchability and compliance, they require a large volume fraction of metallic filler and their Young's modulus (~0.1–1 MPa) is greater than the modulus of soft gels and biological materials (roughly 1–10 kPa), such as adipose (body fat) tissue[19].

Hydrogels are a promising candidate for soft electronics since they have similar mechanical properties to a range of biological materials and soft tissues[20,21], including epidermal skin[22], brain[23], spinal cord[24] and cardiac tissue[25]. Recent research has highlighted various aspects of hydrogels, including high fracture toughness, tissue-like Young's modulus (<10^2 kPa), high water content (>75%), ionic conductivity, bioactivity and biocompatibility[21,26]. These properties enable unique applications in bioelectronics[27] and soft robotics[28], including soft-matter sensors[9,29] and actuators[30]. However, hydrogels have an intrinsic ionic conductivity (10^{-5} to 10^{-1} S cm^{-1}; refs. [31–33]) that is six to nine orders of magnitude lower than the conductivity of metals, and is inadequate for digital and power electronics[34].

To improve their electrical properties, hydrogel matrices have been filled with conductive materials such as metallic fillers (for example, nanowires or micro/nanoparticles)[35–38], carbon-based conductive materials (carbon nanotubes or graphene)[39,40] and intrinsically conducting polymers (for example, poly(3,4-ethylenedioxythiophene) polystyrene sulfonate (PEDOT:PSS) or polyaniline)[3,34,41,42]. These composites demonstrate the potential for engineering hydrogels that are both electrically conductive (~10^{-5}–10^1 S cm^{-1}) and have tissue-like mechanical compliance. However, there is a trade-off between improved electrical conductivity and lowered compliance and deformability in these conductive hydrogel composites. For example, a pure PEDOT:PSS hydrogel[34] has been developed with electrical conductivity of 40 S cm^{-1} but high Young's modulus (~2 MPa) and low maximum strain limit (<35% strain), while a soft graphene hydrogel[40] has been synthesized with favourable mechanical properties (Young's modulus of 50 kPa) but low electrical conductivity (~10^{-4} S cm^{-1}).

In this Article, we report an electrically conductive hydrogel composite that has high electrical conductivity (374 S cm^{-1}), a low Young's modulus (<10 kPa) matching that of soft biomaterials, such as adipose tissue[19], and high stretchability (250% strain). We use a polyacrylamide (PAAm)–alginate hydrogel that is embedded with a low concentration of silver (Ag) flakes. Electrical conductivity is created via a partial dehydration process[34] in which a moderate portion of water is removed to induce percolation and create electrically conductive pathways (Fig. 1a,b). Because the composite has a low concentration of metallic filler, it exhibits only modest hysteresis between loading and unloading cycles. The Ag–hydrogel composite's high conductivity, low Young's modulus, high electrical stability and high stretchability make it a suitable material for applications in soft robotics, bioelectronics and wearable electronics (Fig. 1c, Supplementary Fig. 1 and Supplementary Table 1). We demonstrate the potential applications of this soft conductor by using it in a light-emitting diode circuit that shows high mechanical compliance (Fig. 1d and Supplementary Fig. 2), a stingray-inspired

[1]Soft Machines Lab, Carnegie Mellon University, Pittsburgh, PA, USA. [2]Mechanical Engineering, Carnegie Mellon University, Pittsburgh, PA, USA. [3]Robotics Institute, Carnegie Mellon University, Pittsburgh, PA, USA. [4]Materials Science & Engineering, Carnegie Mellon University, Pittsburgh, PA, USA. [5]These authors contributed equally: Yunsik Ohm, Chengfeng Pan. ✉e-mail: cmajidi@andrew.cmu.edu

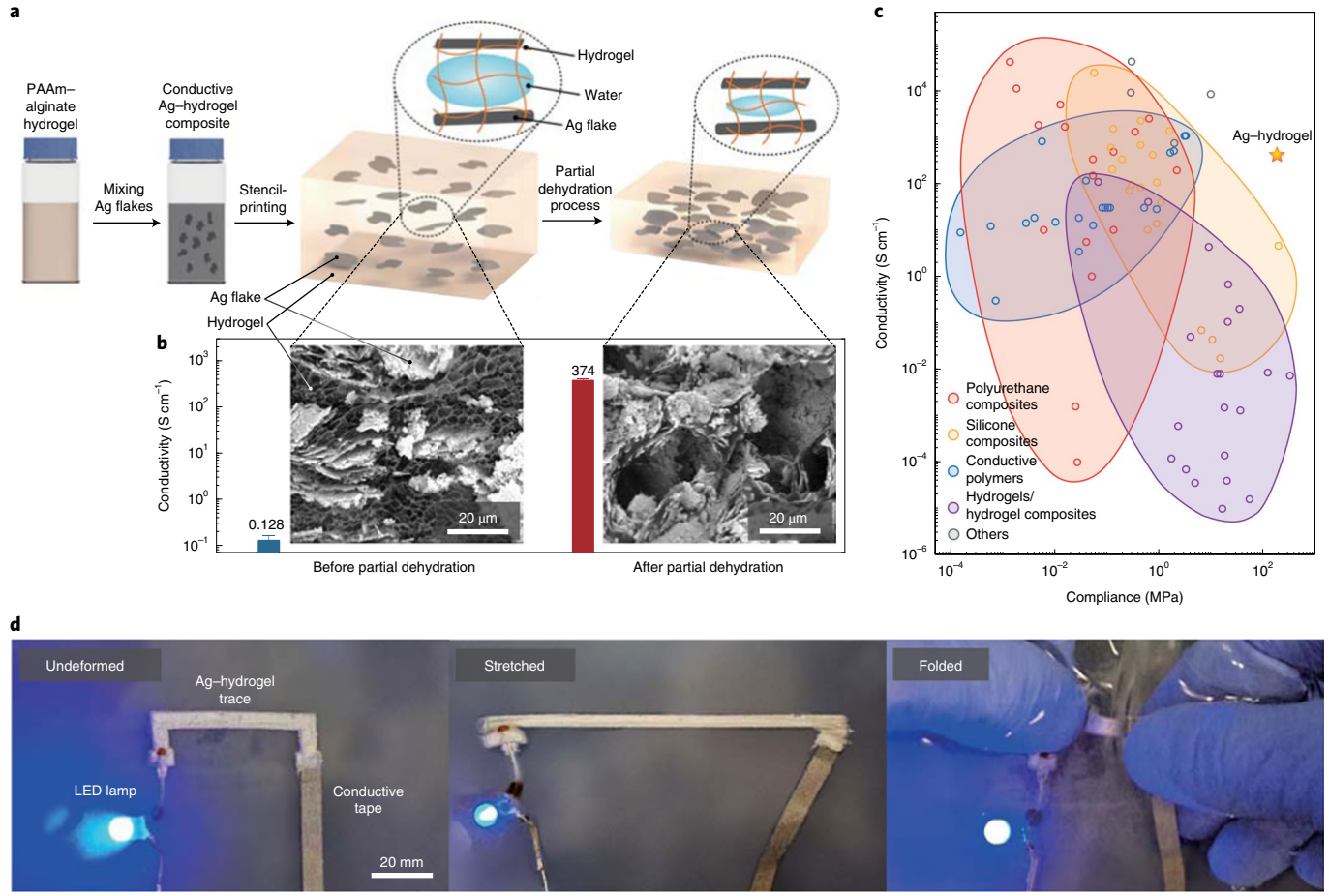

Fig. 1 | Soft, stretchable and electrically conductive hydrogel composite. a, Composition and synthesis of the conductive hydrogel composite composed of micrometre-scale Ag flakes and PAAm–alginate hydrogel (Ag–hydrogel composite). **b**, Conductivity of the Ag–hydrogel composite and micrographs of the composite before and after the controlled partial dehydration process. The error bars are the s.d. for $N = 3$ samples. **c**, An Ashby-style plot comparing conductivity and compliance of the Ag–hydrogel composite with those of other soft conductors (data points are from references mentioned in Supplementary Fig. 1 and Supplementary Table 1). **d**, Undeformed, stretched and folded circuitry made of the stencil-printed Ag–hydrogel composite to power a light-emitting diode (LED) lamp (Supplementary Fig. 2 and Supplementary Video 1).

soft swimmer where the shape-memory alloy (SMA) muscle is actuated with power transmitted through the conductive hydrogel composite, and a neuromuscular electrical stimulation electrode that can deliver high-frequency electrical signals generated by a commercial stimulator.

Ag–hydrogel composite

The highly conductive hydrogel composite was fabricated by controlling the assembly and percolation of Ag flakes within a PAAm–alginate hydrogel matrix. Ag flakes were utilized since silver has high electrical conductivity and the high aspect ratio of the flakes permits morphologies that allow for greater electrical conductivity compared with networks of other conductive particles with similar volume concentration. The key step in achieving high electrical conductivity is to perform a partial dehydration of the hydrogel matrix, which enables the Ag flakes to form percolation pathways that remain stable when the composite is stretched or rehydrated (Fig. 1a). The composition and synthesis of the PAAm–alginate gel matrix was adopted from previous work by Sun et al.[43]. However, for our system, we did not replace the sodium ion (Na^+) of the alginate with other multivalent cations, such as the calcium ion (Ca^{2+}), as had been previously done. Although the material is not ionically crosslinked by multivalent cations, it shows enhanced stretchability and toughness through the formation of a double-network hydrogel matrix enabled by mechanical and chemical interactions between two hydrogel matrices[43,44].

After stencil-printing (Supplementary Fig. 3) and before performing the partial dehydration, the Ag–hydrogel composite is ionically conductive with a low conductivity (~0.13 S cm^{-1}). At this stage of the fabrication process, the volume fraction of the Ag filler (5 vol%) is insufficient for percolation. The reason for using such a low volume fraction of Ag flakes instead of adding enough Ag fillers to exceed the percolation threshold is that the presence of a large amount of Ag will suppress the double crosslinking process of the hydrogel matrix. As observed in cross-section images taken using scanning electron microscopy, adjacent Ag flakes are separated by the surrounding hydrogel matrix and do not form a connected network (Fig. 1b, left). Given that the hydrogel matrix is composed of a hydrophilic polymer network with ~90 vol% of water, partial dehydration reduces the water content and allows for the formation of a percolating network of Ag flakes (Fig. 1b, right, and Supplementary Fig. 4). Concomitantly, we observed that the electrical conductivity of the composite increased from 0.128 S cm^{-1} to 374 S cm^{-1} after dehydration (Fig. 1b). The partial dehydration process enables the hydrogel composite to achieve high electrical conductivity, while maintaining tissue-like mechanical properties, that is, low Young's modulus and high stretchability (Fig. 1c).

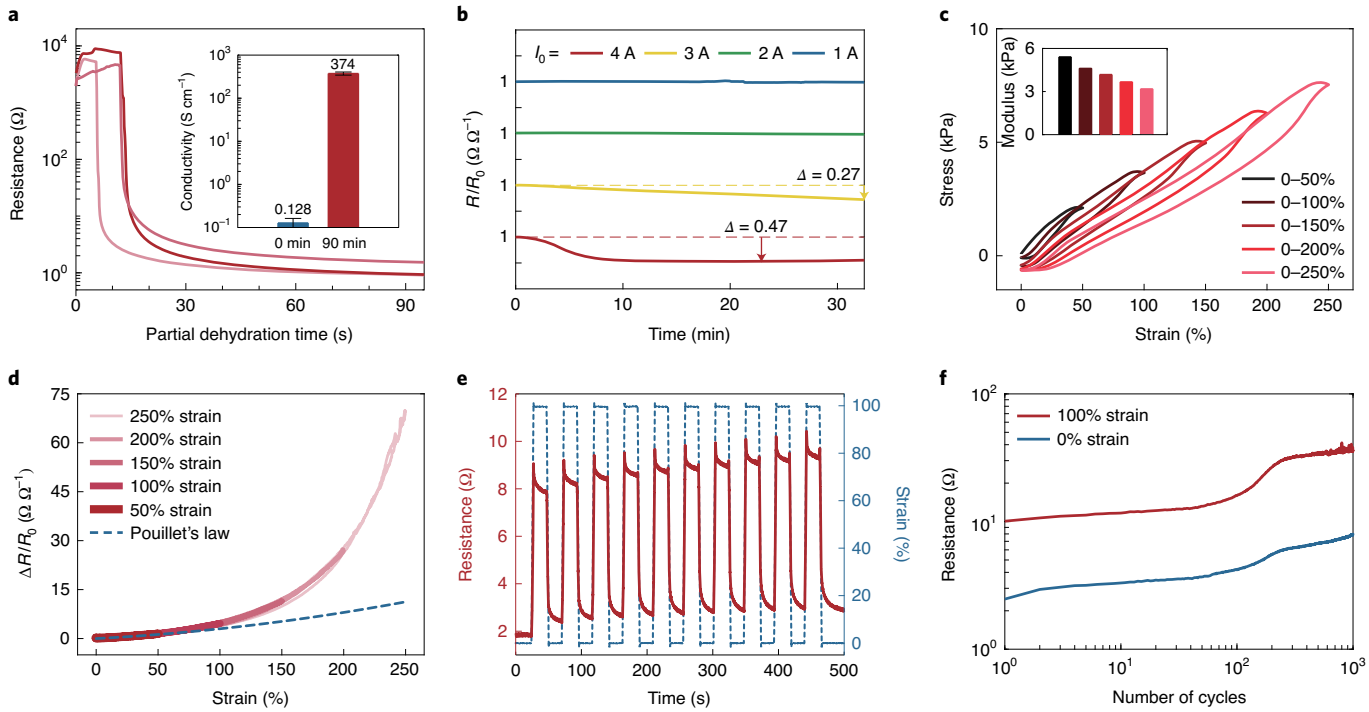

Fig. 2 | Material characterization. a, Absolute change in resistance as a function of time for the partial dehydration process and (inset) the volumetric conductivity at 0 min and 90 min. The error bars are the s.d. for $N=3$ samples. This is for a composite with an initial Ag content of 5 vol%; plots for composites with other initial volume fractions are presented in Supplementary Fig. 5. **b**, Normalized change in resistance as a function of time with different initial currents and corresponding constant voltages; note that a *y*-axis offset is applied to each curve to assist in visualization of the data. Here, Δ is defined as the change in R/R_0 compared to its initial value of 1. **c**, Stress versus strain of the conductive hydrogel composite under different uniaxial loading conditions from 0% to 50%, 100%, 150%, 200% and 250% strain, and effective elastic moduli as a function of loading condition (inset). **d**, Normalized change in resistance as a function of strain (gradient of red solid lines) along with the theoretical prediction using Pouillet's law for an incompressible elastomer with constant volumetric resistivity (dashed blue line). **e**, Electromechanical response as a function of time under uniaxial cyclic loading to 100% strain up to the first 10 cycles. For each cycle, the sample was stretched at 10 mm s^{-1}, held for 20 s, released at 10 mm s^{-1} and held for 20 s. **f**, Cycling stability of the resistance under uniaxial cyclic loading to 100% strain up to 1,000 cycles. The sample was stretched and released at the speed of 10 mm s^{-1}.

We measured electrical resistance changes of the Ag–hydrogel composites with different amounts of Ag in situ during the partial dehydration to better understand the effect of drying (Fig. 2a and Supplementary Fig. 5). The Ag–hydrogel composite specimens (40 mm × 3 mm × 0.7 mm) were stencil-printed on a PAAm–alginate hydrogel substrate using a polydimethylsiloxane mask (Sylgard 184, Dow Corning) (Methods). Figure 2a shows the evolution in resistance as a function of partial drying time and the volumetric conductivity of the composites at 0 min and 90 min for the specimen with an Ag content of 5 vol%. Initially, the resistance was of the order of kiloohms, with a corresponding conductivity of 0.128 ± 0.0348 S cm^{-1} for $N=3$ samples, which indicates no electrical conductivity but ionic conductivity, as the value of conductivity was similar to that of an unfilled hydrogel[45]. The resistance of the Ag–hydrogel composite decreased exponentially after 10–15 min of drying, as electrically conductive paths began to form (Supplementary Fig. 4). As we described previously, Ag flakes do not initially form conductive pathways due to the high initial water content. The evaporation of water in the hydrogel matrix may facilitate intimate contact and adhesion between adjacent Ag flakes and flake aggregates, thereby allowing for the formation of electrically conductive pathways. After exceeding the percolation threshold, the electrical conductivity reaches a saturation plateau. At this stage, the resistance is decreased to $1.14 \pm 0.359\,\Omega$ after 90 min, and the corresponding volumetric conductivity reaches 374 ± 30.8 S cm^{-1} for $N=3$ samples. Higher volumetric Ag content after partial dehydration was observed as the cross-section area of the specimen decreased from 1.76 mm^2 to 1.38 mm^2 after 90 min of drying (Supplementary Fig. 5b), which corresponds to an increase in the effective Ag content from 5.00 vol% to 6.07 vol% and a decrease in the effective water content from 81.9 vol% to 78.1 vol%. Similar trends in resistance during the partial dehydration step were observed for Ag–hydrogel composites with different Ag contents (Supplementary Fig. 5c–f). As the initial Ag content increased, the exponential decrease in resistance occurred more quickly, demonstrating the effect of drying on the electrical conductivity.

Importantly, the percolation network appears to be permanently formed as a result of the dehydration step. When the resistance was recorded in an aqueous environment where it could rehydrate (Supplementary Fig. 6), the Ag–hydrogel composite maintained high electrical conductivity. The resistance was observed to increase after three days in water due to swelling of the hydrogel matrix. However, the percolating network remained largely intact and the absolute resistance was of the same order of magnitude as before rehydration. The absorbed water imposed a capillary force that disrupted the weak conductive pathways of the Ag flakes. However, the main percolating network remained due to the stronger adhesion between contacting flakes (Supplementary Discussion 1 and Supplementary Figs. 7 and 8). In this way, the material was still able to show high electrical conductivity even after being submerged in an aqueous environment for three days (Supplementary Figs. 6 and 9). The results could be compared with an Ag–hydrogel composite that was left in ambient air after partial dehydration, where the resistance decreased slightly (Supplementary Fig. 6). These results

highlight the importance of controlled assembly by dehydration to fabricate the soft conductor.

High electrical conductivity enables the Ag–hydrogel composite to deliver high direct current at low voltages. We first applied a constant voltage and monitored direct current over time for a printed Ag–hydrogel trace which became electrically conductive after the partial dehydration process (Supplementary Fig. 10a). Voltages were applied to give initial current values (I_0) of 1, 2, 3 and 4 A, and the corresponding normalized resistance was also monitored over time (Fig. 2b). For lower currents ($I_0 = 1$ or 2 A), the resistance profiles are stable, which demonstrates the electrical stability of the Ag–hydrogel composite. The resistance gradually decreased when subjected to an initial current of 3 A. When initial direct current of 4 A was applied, we observed a substantial decrease of resistance within 10 min. The decreased resistance saturated at the end of the test. We attribute this resistance decrease to further evaporation of water (beyond the intentional partial dehydration) between adjacent Ag flakes as the composite was heated by Joule heating at high current.

Finite element analysis (FEA) of Joule heating at steady state and the long-term response to high current were compared. The results of simulation (Supplementary Fig. 10c–f) and long-term response to high current (Supplementary Fig. 11) show that the maximum temperature exceeds the boiling point of water (100 °C) when the composite is subjected to an electrical power with an initial current of 3 A or 4 A. This localized high temperature causes bubbles (Supplementary Fig. 12g–l) near the Ag–hydrogel trace and can result in thermal degradation of the hydrogel at 4 A (that is, discolouration of the hydrogel as shown in Supplementary Figs. 12j–l and 13). In contrast, Ag–hydrogel traces subjected to lower electrical currents ($I_0 = 1$ A and 2 A) retain their original appearance (for example, minimal bubbles and no discolouration) due to the lower localized temperature (<100 °C, Supplementary Figs. 10c,d and 11c,d). We further investigated the long-term response of the Ag–hydrogel composite to direct current while underwater. The results in Supplementary Fig. 14 show that the Ag–hydrogel composite can maintain high electrical conductivity in an aqueous environment during long-term usage (Supplementary Discussion 2). These results demonstrate the potential of the Ag–hydrogel composite as a power line for applications in digital electronics that require high direct current and can retain functionality in various environments.

To be mechanically compatible with soft biological tissues, the Ag–hydrogel composite must be highly compliant and deformable. The stress–strain characteristics were evaluated using an Instron 5969 materials testing machine (Fig. 2c). We calculated the effective elastic modulus (Fig. 2c inset) by adopting the hyperelastic constitutive model for a two-parameter Ogden solid[46] and performing a statistical fit ($R^2 = 0.95$). The 5 vol% Ag–hydrogel composite has a modulus of 5–6 kPa after performing partial dehydration (Supplementary Fig. 15), while the unfilled PAAm–alginate hydrogel's modulus is about 3–4 kPa. As observed with other conductive composites[16,40], the introduction of metallic fillers into a soft matrix typically results in a composite with a Young's modulus higher than that of an unfilled matrix. However, since the Ag content is kept low by controlling assembly through the partial dehydration, the Ag–hydrogel composite has tissue-like softness and minimal hysteresis between mechanical loading and unloading.

Conductors that interface with biological tissues typically undergo complex and repetitive deformations, and so it is crucial to understand the electromechanical coupling of the soft conductor. Electromechanical coupling of the Ag–hydrogel composite was measured by monitoring the change in resistance of a stencil-printed composite trace as a function of uniaxial strain. The printed composite was encapsulated with another layer of PAAm–alginate hydrogel after the partial dehydration to prevent further dehydration (Methods). We first examined changes in electrical resistance while subsequently imposing different tensile strains ($\varepsilon = 50$, 100, 150, 200 and 250%; Fig. 2d). The Ag–hydrogel composite was first stretched by 50% strain and then relaxed to its original length, and the strain was increased by 50% up to 250% for each successive cycle. The stretching and releasing curves overlapped, highlighting negligible hysteresis in resistance under different mechanical loading conditions. Since the conductive hydrogel composite shows small mechanical hysteresis, the resistance of the composite also shows small changes under cyclic loadings (Supplementary Fig. 16). In addition, the resistance change at small strain (0–100%) agrees well with Pouillet's law[47], that is, $\Delta R/R_0 = (1+\varepsilon)^2 - 1$, where R is resistance and R_0 is the initial resistance at small strain (0–100%). Moreover, these tests demonstrate that the Ag–hydrogel composite is highly stretchable while maintaining electrical conductivity at strains up to 250%.

Importantly, the composite should be electromechanically robust to multiple strain cycles. Through multiple strain cycles between 0% and 100% strain, the resistance of the Ag–hydrogel composite remains low enough for practical purposes, such as digital circuit functionality or bioelectronics (Fig. 2e). Through 10 loading cycles, the resistance remained relatively constant, with less than 1 Ω change in the relaxed state. When stretched, the electromechanical response was fast, changing according to the mechanical deformation within 0.1 s (Supplementary Fig. 16b,c). While being held directly after stretching for 20 s, the resistance exponentially drops at first; the changes in resistance are about 1.2 Ω and are consistent throughout the 10 cycles. These experiments illustrate the desirable electromechanical features of the Ag–hydrogel composite, which include fast electrical response (20–40 ms when stretched and 160–250 ms when released) to external mechanical stimuli and a robust percolating network for repeatable and consistent elastic response.

To validate long-term use, the Ag–hydrogel composite was also characterized for 1,000 cycles of tensile loading between 0% and 100% strain (Fig. 2f). The resistance at 0% and 100% strain was bounded within stable boundaries for the first 100 cycles, then slightly increased from 2.5 Ω to 4.2 Ω at 0% strain and from 10 Ω to 16 Ω at 100% strain. For subsequent loading cycles, the resistance of the conductive hydrogel composite at 100% strain was observed to increase and then fluctuate when approaching 1,000 cycles. The reason for this fluctuation was that the experiment was conducted in air with a relatively high speed of 10 mm s^{-1}, which led the sample to become drier and stiffer over the duration of the experiment (100 min). This could be avoided by performing the experiment in a humid environment. Nonetheless, the results of electromechanical characterization demonstrate the composite's high conductivity, low electromechanical hysteresis and repeatable electrical response to mechanical deformation.

Stingray-inspired soft swimmer

The tissue-like compliance and deformability of the Ag–hydrogel composite—along with its electrical conductivity—permit its use as a soft conductive material in soft robotics. To demonstrate its potential in soft robotics, we fabricated a stingray-inspired soft swimmer that was composed of a pair of hydrogel pectoral fins and a streamlined backbone made with a soft foam. Two sets of Ag–hydrogel traces formed compatible interfaces with the hydrogel pectoral fins. The soft and conductive traces served as power lines to deliver high current (~3.3 A) from a benchtop power supply (KPS3010D, Eventek) to a pair of SMA actuators without interfering with the natural deformability and compliance of the hydrogel pectoral fin (Fig. 3a). The soft actuators were composed of two SMA wires sandwiched by three layers of Very High Bond (VHB) tape (4905, 3M), which enabled the actuators to bend upwards and downwards alternately through direct Joule heating[48] (Methods). To induce a forward swimming motion, the top pair of SMA wires was activated for 0.6 s and then cooled for 1.9 s while the other pair was activated and cooled for 0.3 and 2.2 s, respectively (Fig. 3b,c). Referring to Fig. 3c, the upward and downward actuation cycles were staggered with a 0.9 s offset period. The stingray-inspired swimmer is capable

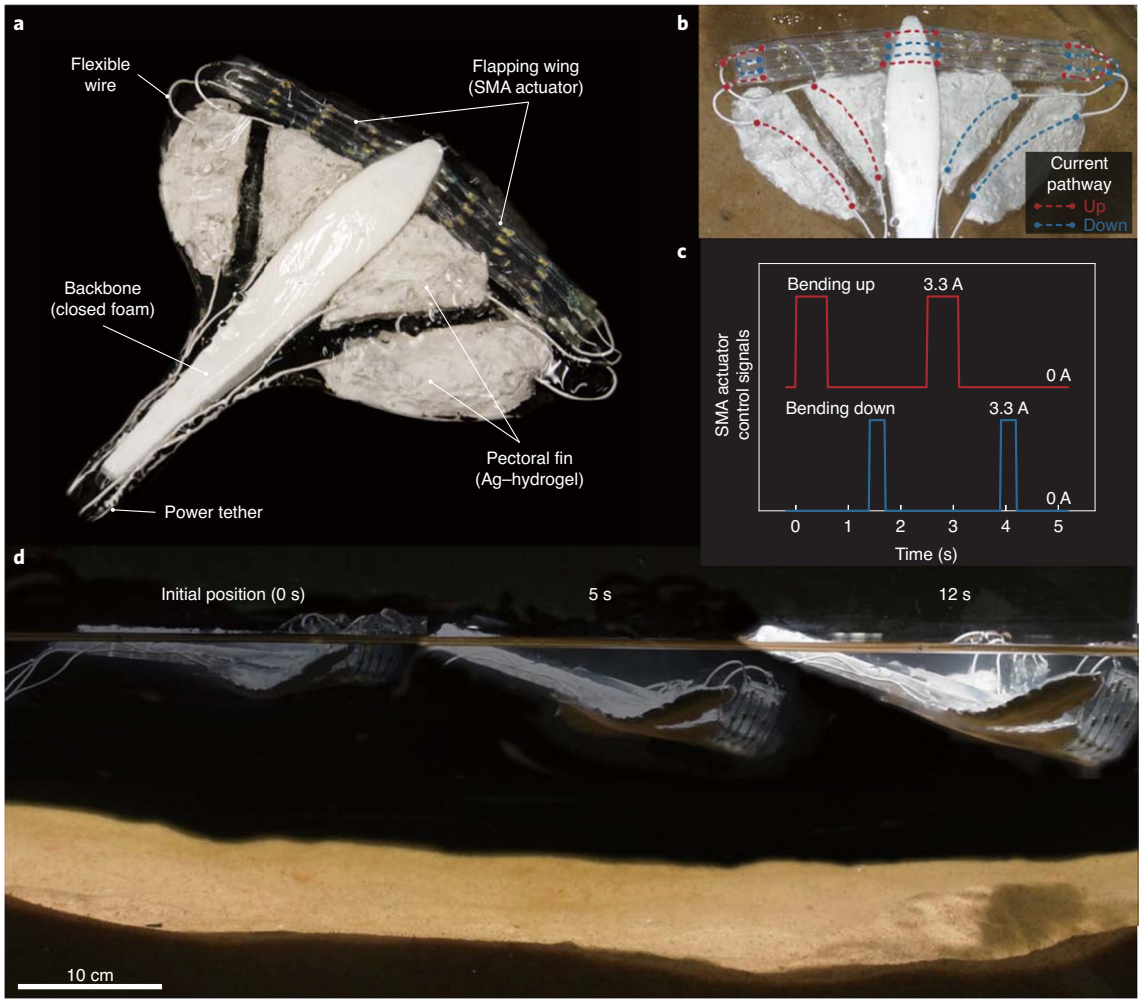

Fig. 3 | Stingray-inspired soft swimmer. a, A soft stingray-inspired swimmer with the conductive hydrogel composite. The soft swimmer is propelled by SMA wires, which require high current (3.3 A) to be actuated and are connected to the tethered power through the conductive hydrogel composite. **b**, Schematic of high-current signal routing, connecting the SMA wires and the power. **c**, Actuation sequence and required current for the soft swimmer. The trace in **b** is colour-coded with reference to **c**. **d**, Sequential images of the soft swimmer from the side view (Supplementary Video 2).

of swimming at an average speed of 0.2 body lengths per second (40 mm s^{-1}) (Fig. 3d and Supplementary Video 2). This demonstration highlights the electrical conductivity and stability of the Ag–hydrogel composite by carrying high currents (3.3 A) to activate the embedded SMA actuators.

Neuromuscular electrical stimulation electrode

The soft and highly conductive Ag–hydrogel composite also has the potential to broaden the utilization of hydrogels as electrodes in the field of epidermal electrical stimulation and recording, which requires electrodes with adequate electrical conductivity[21,49]. Here, we fabricated Ag–hydrogel electrodes to deliver high-frequency electrical signals for neuromuscular electrical stimulation[50] to demonstrate the enabling bioelectronic properties of the composite. As shown in Fig. 4a, a pair of Ag–hydrogel electrodes is connected to a commercial electrical muscle stimulator (PowerDot 2.0 Uno), where the strength and frequency of the pulses are controllable using a smartphone via Bluetooth. For comparison, we also made unfilled hydrogel electrodes with ionic conductivity and performed neuromuscular electrical stimulation under the same conditions (Methods and Supplementary Fig. 17). First, the electrodes stimulate the tibialis anterior muscle of the leg, which dorsiflexes the foot when stimulated (Fig. 4b and Supplementary Video 3). With the same stimulation intensity, we measured the relative change in dorsiflexion angle from the side view (Fig. 4c) and the frequency of vibration (Fig. 4d). Figure 4d shows that the frequencies of muscle stimulation in the two cases are almost identical because the signal was generated by the same device and power. However, as shown in Fig. 4c, the relative changes in dorsiflexion angle are different in the two cases: the Ag–hydrogel electrodes were able to deliver sufficient current to induce dorsiflexion in the foot, whereas the electrodes made of ionic hydrogel appeared ineffective to conduct enough current to contract the muscle. We also compared the performance of the Ag–hydrogel electrodes and commercial electrodes (made by PowerDot) along with the neuromuscular electrical stimulation device, which shows that the Ag–hydrogel electrodes have comparable performance to the commercially available neuromuscular electrical stimulation electrodes (Supplementary Fig. 18). The next experiment was conducted on the muscles in the posterior of the forearm, which results in tremors in the wrist and the fingers curling in towards the palm (Fig. 4e, Supplementary Fig. 17 and Supplementary Video 4). The result shows that the stimulation driven by Ag–hydrogel electrodes exhibits a more substantial angle change between the proximal phalange and the metacarpus of the ring and little fingers compared with the case of ionic hydrogel electrodes. This demonstration suggests that the Ag–hydrogel

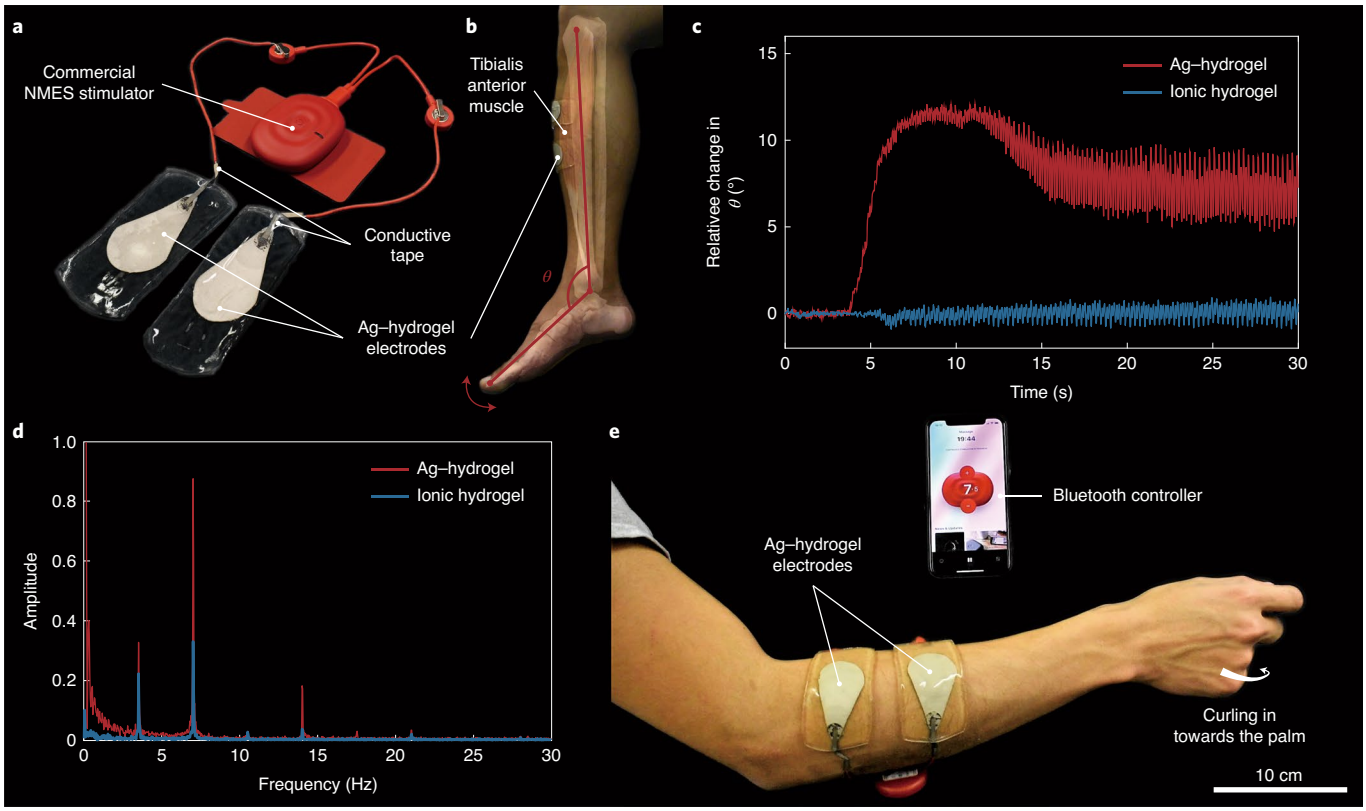

Fig. 4 | Neuromuscular electrical stimulation electrode. a, Neuromuscular electrical stimulation electrodes made of the Ag–hydrogel composite are assembled with a commercial electrical muscle stimulator. **b**, The electrodes are placed on the tibialis anterior muscle of the participant's leg to cause dorsiflexion (Supplementary Video 3). The red lines are used to track the relative change of the angle (θ). **c**, Relative change in dorsiflexion angle as a function of stimulation time. **d**, Amplitude as a function of frequency, which is the result of fast Fourier transform. **e**, The electrodes are placed on the arm and deliver electrical signals from the stimulator to the muscles in the posterior of the forearm (Supplementary Video 4).

composite has the potential to improve bioelectronic interfacing of tissue–electrode contacts due to its high electrical conductivity and soft conformability.

Conclusions

We have reported an Ag–hydrogel composite that is based on two materials with disparate mechanical properties—Ag flakes and hydrogel matrix—and exhibits high electrical conductivity (>300 S cm^{-1}), electrical stability under repeated mechanical loading, low Young's modulus (<10 kPa) and high stretchability (up to 250% strain without electrical failure). To illustrate the capabilities of the Ag–hydrogel composite, we fabricated a stingray-inspired swimmer driven by SMAs that require high current, high compliance and high stretchability for actuation. We also developed skin-mounted electrodes made of the Ag–hydrogel composite for neuromuscular electrical stimulation, which require conformal contact and high conductivity to deliver electrical impulses with high frequency.

This combination of high electrical conductivity and high compliance is achieved by controlling the assembly of Ag inclusions when dispersing the micrometre-sized Ag flakes in the PAAm and alginate hydrogel. A key step in the fabrication process is the partial dehydration step, which allows intimate contact between Ag flakes and the formation of a percolating network that remains intact and stable even as the gel is fully rehydrated. The conductive hydrogel composites also have robust and reliable electromechanical coupling. The combination of electrical and mechanical properties of the Ag–hydrogel composite occupies a unique place in the design space of electrically conductive soft materials (Fig. 1c and Supplementary Fig. 1) and could be of use in the development of soft robotics, bioelectronics and wearable electronics.

Methods

Materials. The chemicals used as components of the hydrogel were dissolved in deionized water (McMaster-Carr). For PAAm gel, 40 wt% acrylamide (AAm, A8887, Sigma-Aldrich) was used as the monomer for the PAAm hydrogel network. *N*,*N*-methylenebisacrylamide (MBAA, 146072, Sigma-Aldrich, 1 wt%) was used as the crosslinker. Ammonium persulfate (APS, A3678, Sigma-Aldrich, 5 wt%) was used for curing hydrogel substrates and 20 wt% APS was used for curing Ag–hydrogel composites. In both cases, APS functions as a thermal or photo-initiator. *N*,*N*,*N*′,*N*′-tetramethylethylenediamine (TEMED, T9281, Sigma-Aldrich, 5 wt%) was used as an accelerator to make the curing process faster. For alginate gel, sodium alginate (W201502, Sigma-Aldrich) was used as the monomer for the alginate hydrogel network. For conductive fillers, micrometre-scale sized Ag flakes (2–5 µm, 47MR-10F, Inframat Advanced Materials) were mixed with the PAAm–alginate hydrogel matrix.

Synthesis of PAAm–alginate hydrogel. We synthesized stretchable and tough hydrogels by mixing linear copolymer alginate and covalently crosslinked PAAm using a method adopted from previous works[43,51]. Unless otherwise stated, the water content of hydrogel was fixed at 86 wt% when the hydrogel was initially cured. We mixed alginate with 40 wt% AAm in water solution with additional deionized water and waited until the alginate was fully dissolved. The ratio of alginate to AAm was 1:6 by weight. When the alginate became fully dissolved, the mixture was mixed with 1 wt% MBAA (0.06% of the total weight of AAm) and 5 wt% TEMED (0.24% of the total weight of AAm). For the last step of the synthesis process, 5 wt% APS (0.75% of the total weight of AAm) was added to cure the hydrogel pre-gel solution. The chemicals used in this process were mixed using a planetary centrifugal mixer at 2,000 r.p.m. (AR-100, Thinky Corporation).

Synthesis of conductive Ag–hydrogel composite. We synthesized a conductive hydrogel composite by mixing the above-mentioned PAAm–alginate hydrogel with micrometre-sized Ag flakes. Ag flakes (5 vol% of the volume of hydrogel) were mixed with the mixture of alginate, deionized water and 40 wt% AAm. This was mixed

once more after adding MBAA and TEMED. However, with the same amounts of chemical components as in the case of PAAm–alginate hydrogel, the mixture was not cured because of the dispersed Ag flakes within the hydrogel pre-gel solution. By increasing the amount of 1 wt% MBAA by a factor of five (corresponding to 0.3% of the total weight of AAm), the crosslinking network between polymer chains was successfully formed in the presence of Ag flakes. Additionally, to increase the curing rate, 20 wt% APS (3% of the total weight of AAm) was used.

Partial dehydration process. We used a digital multimeter (34401A, Keysight Technologies, or 2100, Keithley, Supplementary Fig. 19) with a four-point probe to record the change in resistance of the printed Ag–hydrogel composite (40 mm length, 3 mm width and 0.7 mm thickness) on a 1.6-mm-thick PAAm–alginate hydrogel substrate. EGaIn (75 wt% Ga and 25 wt% In; Solution Materials) was used at each end of the printed trace to minimize contact resistance between the probes and the conductive hydrogel composite. The partial dehydration process proceeded in an acrylic box with holes, where the humidity and temperature of the environment in the box were monitored by a digital sensor (B07HMV6GG2, Linkstyle). The resistance values were manually recorded. These tests were conducted in a laboratory with an air conditioner that set the room temperature around 22 °C.

Volumetric conductivity. The volumetric conductivity ($\sigma = l/RA$) of the printed Ag–hydrogel trace was calculated using an effective trace length ($l = 40$ mm) and effective cross-sectional area ($A = 1.76\,\mu m^2$ for the case before the partial dehydration process and $A = 1.38\,mm^2$ for the case after the partial dehydration process; see Supplementary Fig. 5 for representative sample dimensions). The cross-sectional area was measured using a digital microscope (1000X, MicroTroniX).

Electromechanical characterization. The Ag–hydrogel composite was stencil-printed on a 1.6-mm-thick PAAm–alginate hydrogel. EGaIn was located at each end of the printed trace to minimize contact resistance between the conductive hydrogel composite and the wires from a USB (Universal Serial Bus) data acquisition device (USB-6002, NI), which collects external analogue data from the materials testing machine (5969, Instron) at a rate of 1 kHz. After the partial dehydration process was completed, the printed Ag–hydrogel composite was sealed using PAAm–alginate pre-gel when the resistance reached 2 Ω. After 10 min, the pre-gel solution started to be cured. The samples were cut around the trace using a razor blade and assembled with three-dimensional (3D) printed grips. The data were saved using software (MATLAB, 2016a) that can communicate with the USB data acquisition device.

Electrical stability test. Samples were prepared in the same way as the samples used in electromechanical tests: a printed Ag–hydrogel composite trace within two layers of 1.6-mm-thick PAAm–alginate hydrogel. The samples were directly connected to a benchtop power supply (KPS3010D, Eventek). The power supply was set to supply fixed voltage to generate a pre-defined initial direct current (1, 2, 3 or 4 A). The current values were manually recorded.

FEA simulation of Joule heating. Composites were simulated using SOLIDWORKS (Dassault Systèmes). The geometry of the Ag–hydrogel trace was set as 40 mm × 3 mm × 0.7 mm. The trace was encapsulated between two layers of PAAm–alginate hydrogel with a diameter of 83 mm and a thickness of 1.6 mm. The FEA simulation was conducted using the ANSYS Thermal-Electric toolbox. We set the thermal conductivity of the hydrogel layer and Ag–hydrogel trace at 1.045 W (m °C)$^{-1}$ (ref. [52]) and 25.62 W (m °C)$^{-1}$ (ref. [53]), respectively. Additionally, we used 3.086×10^{-3} Ω cm for the Ag–hydrogel composite's resistivity and 20 Ω cm (ref. [54]) for the PAAm–alginate hydrogel's resistivity. Then, two conditions were applied to the model: (1) voltage conditions and (2) convection conditions. For voltage conditions, a fixed voltage difference was applied to the end of the Ag–hydrogel trace. The value was varied in each case. For convection conditions, we used 'Stagnant Air—Simplified Case' at 22 °C with a heat transfer coefficient of 5 W (m^2 °C)$^{-1}$. This condition is applied to the top surface of the additional layer of PAAm–alginate hydrogel and to the sides of the sample. We also set a constant temperature of 22 °C on the bottom of the sample as a boundary condition.

Mechanical characterization. Samples were prepared in a dogbone shape (Die A, ASTM D412) and tested on a materials testing machine (5969, Instron) at a strain rate of 20 mm min^{-1}, unless otherwise stated. Each sample was cured in a 5-mm-thick polyacrylate mould that was printed using a 3D printer (Objet24, Stratasys). After fabrication (Synthesis of conductive Ag–hydrogel composite), samples were clamped using self-tightening roller grips (2713-001, Instron). Two different types of sample were tested: (1) PAAm–alginate hydrogel without conductive fillers and (2) Ag–hydrogel composite.

Environmental stability test. Samples were prepared in the same way as the samples used in electromechanical tests and electrical stability tests. The resistance of the trace was measured using a digital multimeter (34420A, HP) with a four-point probe. The data were collected using a script in MATLAB (2016a, MathWorks). For the ambient air experiment, the samples were left unattended without any additional treatment for three days. Otherwise, for the water experiment, the samples were contained in glass beakers. After initial set-up to measure the resistance, deionized water was added to submerge the trace using a disposable plastic pipette. During the three-day test, deionized water was properly resupplied to maintain the aqueous environment.

Stingray-inspired soft-swimmer fabrication. We started fabrication of the stingray-inspired swimmer by laser-cutting the soft closed foam into a streamlined shape. Then we cut a rectangular through-hole on the side of the streamlined body so that the actuators could be inserted through it. The actuator was composed of four nitinol wires (0.38 mm in diameter; Dynalloy) that were trained to curled shapes by fixing them on aluminium cylinder moulds and baking in an oven for 25 min at 500 °C along with a quenching process. Each pair of trained nitinol wires was connected with a small piece of ultraflexible wire (9564T1, McMaster-Carr) and placed on top of a rectangular VHB tape (80 mm × 20 mm × 0.5 mm, 4905, 3M) with the bending direction facing downwards. Next, the nitinol wires with the VHB tapes were placed on both sides of a rectangular VHB tape with the same dimensions. After the assembly, the actuator was capable of bending both upwards and downwards by direct Joule heating. After this, we connected two actuators with the ultraflexible wires and nitinol wires with the same bending direction were connected in series. The actuators were inserted through the rectangular hole on the backbone with the identical length and angle extruded (Supplementary Fig. 20a). Finally, the backbone and the actuators were placed in a 3D printed mould that was lined with a cured thin layer of PAAm–alginate hydrogel. The Ag–hydrogel composite was stencil-printed into the shape of pectoral fins along the outline of the mould (Supplementary Fig. 20b). At the end of each line of the conductive hydrogel, ultraflexible wire was embedded and connected to the wire of the SMA actuators. The other end of the flexible wire was soldered with another long wire to connect with an external control board. When the Ag–hydrogel composite achieved a certain conductivity (Partial dehydration process), additional pre-gel PAAm–alginate was poured on top of the assembled components. After the additional hydrogel was cured, the swimmer was gently detached from the mould in an aqueous environment.

Neuromuscular electrical stimulation electrode fabrication. We made two versions of neuromuscular electrical stimulation electrodes: (1) electrodes made of the electrically conductive Ag–hydrogel composite and (2) electrodes made of ionically conductive PAAm–alginate hydrogel. First, we made a 1.6-mm-thick PAAm–alginate hydrogel substrate. When the substrate was crosslinked, the conductive tape was placed on the substrate as an electrical bridge between a commercial neuromuscular electrical stimulator (PowerDot) and neuromuscular electrical stimulation eletrodes. A thin layer of EGaIn was deposited on the conductive tape as a soft conductor to minimize the contact resistance. For the case of Ag–hydrogel electrodes, the conductive hydrogel composite was stencil-printed on top of the substrate and the conductive tape. After this, a pre-gel solution of PAAm–alginate hydrogel was poured on the very top as the second layer of the electrodes. In this step, for the conductive hydrogel composite version, a certain amount of time was required to wait for the material to be electrically conductive. The electrode can be cut into desirable form factors for specific muscles using a razor blade (Supplementary Fig. 17a). To connect the electrodes to the stimulator, each electrode was soldered with a wire that electrically connected with a magnet at the end of it (Fig. 4a). The electrodes and the stimulator can be connected though the magnet without compromising the electrical properties. The authors obtained research participants' consent beforehand.

Motion analysis of neuromuscular electrical stimulation. To quantify the muscle stimulation response, videos were recorded using a Nikon D5600 camera at a frame rate of 60 Hz. For the lower-limb stimulation videos, we developed a customized tracking algorithm to locate the end points of the tibia and the toe in every frame by template matching of skin features to calculate the dorsiflexion angle. The reference line of the tibia is defined by its two end points, whereas the reference line of the foot is defined by the lower end point of the tibia and the toe, assuming that flexion of the latter is negligible. The reference lines were used to calculate the change in dorsiflexion angle relative to its initial position, taken as the average from the first second. The two videos with the Ag–hydrogel composite and ionic hydrogel are synchronized using the starting point of the PowerDot stimulation program.

Reporting Summary. Further information on research design is available in the Nature Research Reporting Summary linked to this article.

Data availability

The data that support the plots within this paper and the other findings of this study are available from the corresponding author upon reasonable request.

Code availability

The customized tracking algorithm used in this work is available at https://doi.org/10.1184/R1/14039801.

Received: 6 May 2020; Accepted: 25 January 2021;
Published online: 1 March 2021

References

1. Lin, S. et al. Stretchable hydrogel electronics and devices. *Adv. Mater.* **28**, 4497–4505 (2015).
2. Schiavone, G. et al. Soft, implantable bioelectronic interfaces for translational research. *Adv. Mater.* **32**, 1906512 (2020).
3. Pan, L. et al. Hierarchical nanostructured conducting polymer hydrogel with high electrochemical activity. *Proc. Natl Acad. Sci. USA* **109**, 9287–9292 (2012).
4. Dejace, L., Laubeuf, N., Furfaro, I. & Lacour, S. P. Gallium-based thin films for wearable human motion sensors. *Adv. Intell. Syst.* **1**, 1900079 (2019).
5. Qiu, T., Palagi, S., Sachs, J. & Fischer, P. Soft miniaturized linear actuators wirelessly powered by rotating permanent magnets. In *Proc. IEEE International Conference on Robotics and Automation* 3595–3600 (IEEE, 2018).
6. Zhang, W., Feng, P., Chen, J., Sun, Z. & Zhao, B. Electrically conductive hydrogels for flexible energy storage systems. *Prog. Polym. Sci.* **88**, 220–240 (2019).
7. Shi, Y. & Yu, G. Designing hierarchically nanostructured conductive polymer gels for electrochemical energy storage and conversion. *Chem. Mater.* **28**, 2466–2477 (2016).
8. Larson, C. et al. Highly stretchable electroluminescent skin for optical signalling and tactile sensing. *Science* **351**, 1071–1074 (2016).
9. Kim, C.-C., Lee, H.-H., Oh, K. H. & Sun, J.-Y. Highly stretchable, transparent ionic touch panel. *Science* **353**, 682–687 (2016).
10. Kim, J. et al. Battery-free, stretchable optoelectronic systems for wireless optical characterization of the skin. *Sci. Adv.* **2**, e1600418 (2016).
11. Lee, W. et al. Integration of organic electrochemical and field-effect transistors for ultraflexible, high temporal resolution electrophysiology arrays. *Adv. Mater.* **28**, 9722–9728 (2016).
12. Lin, Y. et al. Vacuum filling of complex microchannels with liquid metal. *Lab Chip* **17**, 3043–3050 (2017).
13. Koh, A. et al. A soft, wearable microfluidic device for the capture, storage, and colorimetric sensing of sweat. *Sci. Transl. Med.* **8**, 366ra165 (2016).
14. Pan, C. et al. Silver-coated poly(dimethylsiloxane) beads for soft, stretchable, and thermally stable conductive elastomer composites. *ACS Appl. Mater. Interfaces* **11**, 42561–42570 (2019).
15. Tavakoli, M. et al. EGaIn-assisted room-temperature sintering of silver nanoparticles for stretchable, inkjet-printed, thin-film electronics. *Adv. Mater.* **30**, 1801852 (2018).
16. Wang, J. et al. Printable superelastic conductors with extreme stretchability and robust cycling endurance enabled by liquid-metal particles. *Adv. Mater.* **30**, 1706157 (2018).
17. Markvicka, E. J., Barlett, M. D., Huang, X. & Majidi, C. An autonomously electrically self-healing liquid metal–elastomer composite for robust soft-matter robotics and electronics. *Nat. Mater.* **17**, 618–624 (2018).
18. Fassler, A. & Majidi, C. Liquid-phase metal inclusions for a conductive polymer composite. *Adv. Mater.* **27**, 1928–1932 (2015).
19. Comley, K. & Fleck, N. A. A micromechanical model for the Young's modulus of adipose tissue. *Int. J. Solids Struct.* **47**, 2982–2990 (2010).
20. Keplinger, C. et al. Stretchable, transparent, ionic conductors. *Science* **341**, 984–987 (2013).
21. Yuk, H., Lu, B. & Zhao, X. Hydrogel bioelectronics. *Chem. Soc. Rev.* **48**, 1642–1667 (2019).
22. Kim, D.-H. et al. Epidermal electronics. *Science* **333**, 838–843 (2011).
23. Kim, D.-H. et al. Dissolvable films of silk fibroin for ultrathin conformal bio-integrated electronics. *Nat. Mater.* **9**, 511–517 (2010).
24. Minev, I. R. et al. Electronic dura mater for long-term multimodal neural interfaces. *Science* **347**, 159–163 (2015).
25. Xu, L. et al. 3D multifunctional integumentary membranes for spatiotemporal cardiac measurements and stimulation across the entire epicardium. *Nat. Commun.* **5**, 3329 (2014).
26. Erol, O., Pantula, A., Liu, W. & Gracias, D. H. Transformer hydrogels: a review. *Adv. Mater. Technol.* **4**, 1900043 (2019).
27. Han, L. et al. A mussel-inspired conductive, self-adhesive, and self-healable tough hydrogel as cell stimulators and implantable bioelectronics. *Small* **13**, 1601916 (2016).
28. Palagi, S. et al. Structured light enables biomimetic swimming and versatile locomotion of photoresponsive soft microrobots. *Nat. Mater.* **15**, 647–653 (2016).
29. Lopes, P. A. et al. Soft bioelectronic stickers: selection and evaluation of skin-interfacing electrodes. *Adv. Healthc. Mater.* **8**, 1900234 (2019).
30. Yuk, H. et al. Hydraulic hydrogel actuators and robots optically and sonically camouflaged in water. *Nat. Commun.* **8**, 14230 (2017).
31. Yang, C. & Suo, Z. Hydrogel ionotronics. *Nat. Rev. Mater.* **3**, 125–142 (2018).
32. Lee, H.-R., Kim, C.-C. & Sun, J.-Y. Stretchable ionics—a promising candidate for upcoming wearable devices. *Adv. Mater.* **30**, 1704403 (2018).
33. Rivnay, J., Wang, H., Fenno, L., Deisseroth, K. & Malliaras, G. G. Next-generation probes, particles, and proteins for neural interfacing. *Sci. Adv.* **3**, e1601649 (2017).
34. Lu, B. et al. Pure PEDOT:PSS hydrogels. *Nat. Commun.* **10**, 1043 (2019).
35. Dvir, T. et al. Nanowired three-dimensional cardiac patches. *Nat. Nanotechnol.* **6**, 720–725 (2011).
36. Ahn, Y., Lee, H., Lee, D. & Lee, Y. Highly conductive and flexible silver nanowire-based microelectrodes on biocompatible hydrogel. *ACS Appl. Mater. Interfaces* **6**, 18401–18407 (2014).
37. Lim, C. et al. Stretchable conductive nanocomposite based on alginate hydrogel and silver nanowires for wearable electronics. *APL Mater.* **7**, 031502 (2019).
38. Jing, X. et al. Stretchable gelatin/silver nanowires composite hydrogels for detecting human motion. *Mater. Lett.* **237**, 53–56 (2019).
39. Shin, S. R. et al. Carbon-nanotube-embedded hydrogel sheets for engineering cardiac constructs and bioactuators. *ACS Nano* **7**, 2369–2380 (2013).
40. Jo, H. et al. Electrically conductive graphene/polyacrylamide hydrogels produced by mild chemical reduction for enhanced myoblast growth and differentiation. *Acta Biomater.* **48**, 100–109 (2017).
41. Zhao, W., Han, Z., Ma, L., Sun, S. & Zhao, C. Highly hemo-compatible, mechanically strong, and conductive dual cross-linked polymer hydrogels. *J. Mater. Chem. B* **4**, 8016–8024 (2016).
42. Feig, V. R. et al. Mechanically tunable conductive interpenetrating network hydrogels that mimic the elastic moduli of biological tissue. *Nat. Commun.* **9**, 2740 (2018).
43. Sun, J.-Y. et al. Highly stretchable and tough hydrogels. *Nature* **489**, 133–136 (2012).
44. Yang, C. H. et al. Strengthening alginate/polyacrylamide hydrogels using various multivalent cations. *ACS Appl. Mater. Interfaces* **5**, 10418–10422 (2013).
45. Mondal, S., Das, S. & Nandi, A. K. A review on recent advances in polymer and peptide hydrogels. *Soft Matter* **16**, 1404–1454 (2020).
46. Ogden, R. W. Large deformation isotropic elasticity—on the correlation of theory and experiment for incompressible rubberlike solids. *Rubber Chem. Technol.* **46**, 398–416 (1973).
47. Kim, H. J., Son, C. & Ziaie, B. A multiaxial stretchable interconnect using liquid-alloy-filled elastomeric microchannels. *Appl. Phys. Lett.* **92**, 011904 (2008).
48. Huang, X., Kumar, K., Jawed, M. K., Ye, Z. & Majidi, C. Soft electrically actuated quadruped (SEAQ)—integrating a flex circuit board and elastomeric limbs for versatile mobility. *IEEE Robot. Autom. Lett.* **4**, 2415–2422 (2019).
49. Li, H., Erbaş, A., Zwanikken, J. & Cruz, M. O. D. L. Ionic conductivity in polyelectrolyte hydrogels. *Macromolecules* **49**, 9239–9246 (2016).
50. Lake, D. A. Neuromuscular electrical stimulation. *Sports Med.* **13**, 320–336 (1992).
51. Yuk, H., Zhang, T., Lin, S., Parada, G. A. & Zhao, X. Tough bonding of hydrogels to diverse non-porous surfaces. *Nat. Mater.* **15**, 190–196 (2016).
52. Xu, S., Cai, S. & Liu, Z. Thermal conductivity of polyacrylamide hydrogels at the nanoscale. *ACS Appl. Mater. Interfaces* **10**, 36352–36360 (2018).
53. Hugh, D. Y. & Freedman, R. A. *University Physics* (Addison-Wesley, 1992).
54. Thibodeau, J. & Ignaszak, A. Flexible electrode based on MWCNT embedded in a cross-linked acrylamide/alginate blend: conductivity vs. stretching. *Polymers* **12**, 181 (2020).

Acknowledgements

We acknowledge support from the NOPP Award (N000141812843; Research Collaborator R. Beach). We thank S. Kim for help with the FEA simulation of Joule heating using ANSYS software.

Author contributions

Y.O., C.P., M.J.F., X.H., J.L. and C.M. designed the research; Y.O. and C.P. fabricated the materials; Y.O., C.P. and M.J.F. performed the experiments; Y.O., C.P., M.J.F., J.L. and C.M. analysed the data; Y.O., C.P. and X.H. produced the demonstration of the soft stingray-inspired swimmer; Y.O., C.P. and J.L. demonstrated the neuromuscular electrical stimulation electrodes; Y.O., C.P., M.J.F., X.H., J.L. and C.M. wrote the manuscript. Y.O., C.P., M.J.F. and C.M. revised the manuscript.

Competing interests

The authors declare no competing interests.

Additional information

Supplementary information The online version contains supplementary material available at https://doi.org/10.1038/s41928-021-00545-5.

Correspondence and requests for materials should be addressed to C.M.

Peer review information *Nature Electronics* thanks Guo Zhan Lum, Shaoting Lin and the other, anonymous, reviewer(s) for their contribution to the peer review of this work.

Reprints and permissions information is available at www.nature.com/reprints.

Publisher's note Springer Nature remains neutral with regard to jurisdictional claims in published maps and institutional affiliations.